Magnetoresistance and Charge Transport in Graphene Governed by Nitrogen Dopants

Markus Rein,[†,§] Nils Richter,[†,§] Khaled Parvez,[‡] Xinliang Feng,[∥] Hermann Sachdev,[‡] Mathias Kläui,[*,†] and Klaus Müllen[‡]

[†]Institut für Physik, Johannes Gutenberg-Univsersity, 55128 Mainz, Germany, [‡]Max Planck Institute for Polymer Research, 55128 Mainz, Germany, and [∥]Molecular Functional Materials, Dresden University of Technology, 01069 Dresden, Germany. [§]These authors contributed equally.

ABSTRACT We identify the influence of nitrogen-doping on charge- and magnetotransport of single layer graphene by comparing doped and undoped samples. Both sample types are grown by chemical vapor deposition (CVD) and transferred in an identical process onto Si/SiO_2 wafers. We characterize the samples by Raman spectroscopy as well as by variable temperature magnetotransport measurements. Over the entire temperature range, the charge transport properties of all undoped samples are in line with literature values. The nitrogen doping instead leads to a 6-fold increase in the charge carrier concentration up to 4×10^{13} cm^{-2} at room temperature, indicating highly effective doping. Additionally it results in the opening of a charge transport gap as revealed by the temperature dependence of the resistance. The magnetotransport exhibits a conspicuous sign change from positive Lorentz magnetoresistance (MR) in undoped to large negative MR that we can attribute to the doping induced disorder. At low magnetic fields, we use quantum transport signals to quantify the transport properties. Analyses based on weak localization models allow us to determine an orders of magnitude decrease in the phase coherence and scattering times for doped samples, since the dopants act as effective scattering centers.

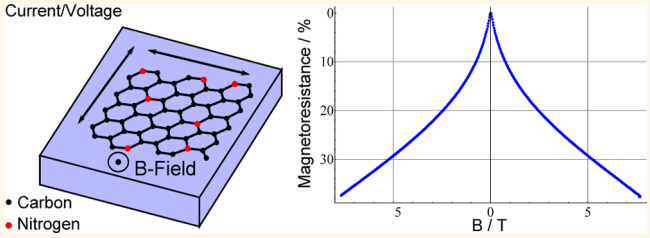

KEYWORDS: CVD graphene · nitrogen doping · negative magnetoresistance · weak localization

Graphene's exceptional charge transport properties qualify it as a promising candidate for future electronic devices.[1−3] To reach this goal, the electronic properties must be engineered to meet device demands such as specific charge carrier mobilities, specific charge carrier densities, or engineered band gaps.

Adatoms and defects have been reported to be a powerful tool to manipulate such properties.[4−13] A variety of dopants have been suggested, ranging from ozone to fluorine.[14,15] The comparison of electronic properties of doped graphene to those of undoped graphene fabricated by the same method has not been reported yet. However, if graphene with and without dopants is produced by different fabrication routes, differences in the transport properties cannot be unambiguously attributed soley to the dopants. It is well-known that graphene, produced by different methods, may exhibit very different charge transport properties. Samples produced by mechanical exfoliation, chemical vapor deposition (CVD) *etc.* show different charge carrier densities and different mobilities resulting from the different growth and handling protocols.[16] Consequently only a combined study with nominally identically fabricated and handled graphene samples with and without nitrogen doping allows one to determine the pure effect of nitrogen and check if this dopant can provide the required tailoring of the electronic properties. Furthermore, up to now adatoms were generally induced using laboratory-based methods which do not allow for any upscaling, neither of the sample dimensions nor of the sample production. The growth of graphene *via* CVD on the other hand, where impurity atoms are directly incorporated into the lattice with variable densities, offers an industrially compatible route to gain control over this manipulation process.[17,18] Finally the charge transport in magnetic fields is expected to depend on doping as phase coherent transport and magnetoresistance effects

* Address correspondence to klaeui@uni-mainz.de.

Received for review October 7, 2014 and accepted December 30, 2014.

Published online December 30, 2014
10.1021/nn5057063

are highly sensitive to scattering, and so far magnetotransport in samples with well-controlled doping has not been probed systematically.

In this paper we investigate CVD-grown graphene where carbon atoms are replaced by nitrogen atoms and compare it to pristine graphene fabricated by the same method. The doping leads to significantly altered electric transport properties. We observe a transition from positive to negative magnetoresistive behavior, without any sign of saturation, up to fields of 8 T. Measurements of the magnetoresistance, the sheet resistance, and Hall voltages are performed at variable temperatures down to 2.3 K and variable magnetic fields up to 8 T. We furthermore observe quantum transport at low temperatures with strongly reduced coherence times for doped graphene. Combined with the strongly modified mobility this allows us to gauge to what extent the dopants act as scattering centers and allow for tailoring of the charge carrier transport properties.

RESULTS AND DISCUSSION

The structural characterization of the graphene films is performed following their transfer from copper to Si/SiO_2 substrates. This provides an understanding of the effects of the transfer process on the material, such as the generation of ripples. Raman spectroscopy is a suitable tool for this purpose since, for instance, the number of layers can be deduced from the intensity ratio of the 2D peak and the G peak,[19−21] which is directly influenced by the charge carrier density in the sample.[22] A comparison of the Raman spectra for both doped and undoped samples is presented in Figure 1. In the undoped case the 2D peak is nearly twice as high as the G peak. However, since the so-called defect peak at a wavelength of 1350 cm^{-1} shows a low intensity and the D′ peak is missing, we can assume that there is no significant unintentional doping of the sample. The shape of the 2D peak on the other hand confirms the monolayer-structure of the sample as one Lorentzian function describes the Raman signal best, compared to a superposition of multiple Lorentzians, which would indicate a multilayer structure.[23−25] For the nitrogen-doped sample, the intensity ratio of G and 2D modes $I(2D)/I(G)$ of about 0.5 shows the effective doping with nitrogen. The D mode, which indicates different defects as adatoms, substitutes, and vacancies, is increased significantly as a consequence and the D′ peak appears.[26] Finally the shape of the 2D band again allows us to conclude that a single layer structure is maintained after the transfer process without significant ripples or folding.

Next we investigate the transport properties. The values for the charge carrier mobility μ and the charge carrier density n are derived from Hall measurements and are given by

$$n = \frac{1}{R_H \cdot e}, \quad \mu = \frac{1}{e \cdot \rho_s \cdot n} \qquad (1)$$

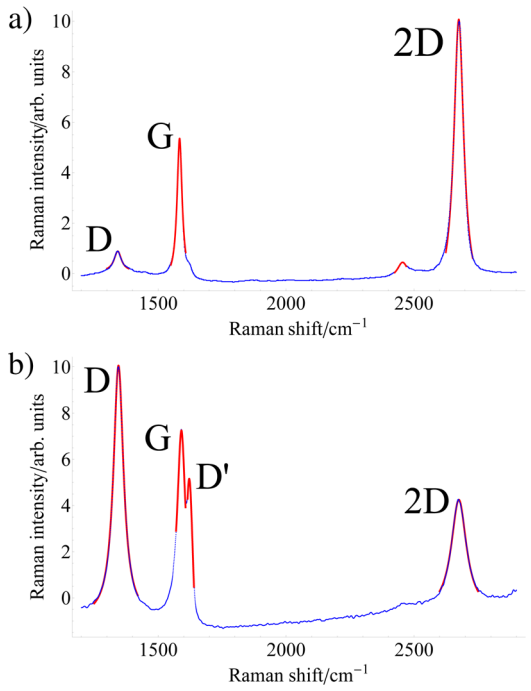

Figure 1. Raman spectrum for undoped graphene (a) and nitrogen-doped graphene (b). The larger defect peak (D) in (b) and the D′ peak indicate an increase of scattering centers due to doping with nitrogen.

where R_H is the Hall constant derived from the slope of the Hall resistance as a function of the applied magnetic field, ρ_s is the sheet resistance and e is the elementary charge. Before comparing the charge transport properties for the doped and undoped CVD graphene, we note that the SiO_2 substrate can affect the mobility and the charge carrier density of the observed devices, *e.g.*, due to surface roughness or charge puddles.[27,28] Without nitrogen doping, we find a charge carrier mobility of (1014 ± 4) $cm^2/(V\,s)$ and a charge carrier density of (6.42 ± 0.03) × 10^{12} cm^{-2} at 279 K. At 2.5 K the mobility amounts to (1122 ± 32) $cm^2/(V\,s)$ and the density to (6.22 ± 0.03) × 10^{12} cm^{-2}. These nearly temperature-independent values are typical for good quality transferred graphene in line with what has previously been reported.[29−31] In case of the nitrogen-doped sample, at 279 K the mobility of (23 ± 4) $cm^2/(V\,s)$ is strongly reduced, whereas the charge carrier density of (39.25 ± 0.15) × 10^{12} cm^{-2}, is strongly increased by more than a factor six compared to the undoped case. For the low-temperature measurement at 2.5 K the resulting values are (11 ± 3) $cm^2/(V\,s)$ and (22.00 ± 0.15) × 10^{12} cm^{-2} respectively. Those observations can be readily explained by the doping: The modification of the graphene lattice with additional nitrogen atoms increases the charge carrier density significantly as each nitrogen atom provides an additional electron. Furthermore, these defects form additional scattering centers and decrease the mobility.

Finally the temperature dependence of the charge carrier density and the mobility in the doped case

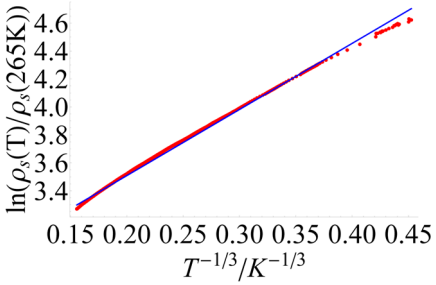

Figure 2. Arrhenius plot of the temperature dependence of the sheet resistance in nitrogen-doped sample. A fit (blue line) of Mott's 2D variable range hopping model to the data allows to extract the activation energy E_0 = (9.11 ± 0.05) meV. At temperatures below a few Kelvin the sheet resistance deviates from the exponential behavior and becomes logarithmic, which indicates phase coherent transport and weak localization.

compared to the undoped case point to the presence of a band gap created by the nitrogen dopants as previously predicted and observed for doped graphene.[17,32,33] Figure 2 shows the sheet resistance as a function of temperature. A clear exponential behavior can be seen over nearly the entire temperature range, which is typical for a semiconducting material. The resistivity in a strongly disordered, *d*-dimensional system is proportional to an exponential factor, which contains the activation temperature T_0 for electron transport:[34]

$$\rho_s(T) \sim \exp[(T_0/T)^{1/(d+1)}] \quad (2)$$

This model adequately describes our observation if we assume a 2D system. In agreement with literature[14] we hereby confirm the 2D nature of the material. With the help of eq 2 we can extract T_0 = (105.8 ± 0.6) K and E_0 = (9.11 ± 0.05) meV, for the activation energy E_0 in nitrogen-doped graphene, which is also in line with the results found for ozone-treated graphene.[14]

The magnetoresistance in nonmagnetic materials is a sensitive tool to study scattering, intrinsic time scales, and phase coherence of the charge transport. So to quantify the transport, we study the magnetoresistance (MR) defined as

$$\mathrm{MR}(B) = \frac{\rho_{\mathrm{sheet}}(B) - \rho_{\mathrm{sheet}}(0)}{\rho_{\mathrm{sheet}}(0)} \quad (3)$$

where $\rho_{\mathrm{sheet}}(B)$ is the sheet resistance at a given magnetic field B. For the undoped graphene a positive MR, see Figure 3a, is found with a small peak for the low-temperature measurement at fields smaller than 0.5 T. The positive high-field part of the MR at both 2.3 and 279 K is well described by the Lorentz magnetoresistance developed by M. Kohler:[35]

$$\mathrm{MR} \sim (\omega_c \tau)^{\alpha} \quad (4)$$

with ω_c the cyclotron frequency, τ the scattering time, and α = 2, in line with previous measurements[36] on pristine graphene on SiO_2. The resulting fit is presented in Figure 3a,b. Similar to the transport properties determined above, there is little change of the high-field MR with temperature, which is due to the nature of the massless charge carriers in undoped graphene. However, the small positive MR peak at low fields (<0.5 T) is visible only at low temperatures. This indicates the phase coherent transport phenomenon of weak localization, which is prominent only at low temperatures and which we discuss further below.

Nitrogen-doped graphene exhibits a very different magnetoresistance signal with the opposite sign as shown in Figure 3c,d. The negative magnetoresistance is detected at all observed fields and at temperatures of 279 and 2.6 K. Both the slope and magnitude of the MR increase at lower temperatures. At 279 K the sheet resistance at zero field is $\rho_{\mathrm{sheet}}(0\ \mathrm{T})$ = 7 kΩ, and we find a 4% decrease (MR) at 8 T. At 2.6 K the sheet resistance amounts to $\rho_{\mathrm{sheet}}(0\ \mathrm{T})$ = 36 kΩ with a much larger decrease of 38% (MR) at 8 T. This observation of negative MR and a strong temperature dependence shows, strikingly, that the nitrogen doping completely changes the nature of the transport.

The decrease at small fields can be attributed to weak localization as seen in the low temperature measurement of the undoped sample. Since this effect only occurs at low temperatures and saturates for magnetic fields <0.5 T, it cannot describe the data over the entire field range, and we discuss this effect further below.

To understand the negative MR at high fields that originates unambiguously from the doping, we compare our experimental data to different theories that model the MR.

The first approach to explain negative MR is the magnetic polaron model.[37,38] Dopant atoms can lead to the formation of local magnetic moments. The interaction of these in combination with Mott range hopping results in different predictions for the MR, depending on the mechanism of interaction between the spins.[38] For our case of a continuous sheet carbon-based system with N dopants we can assume non-interacting spins. In this case, however, this model predicts an opposite temperature dependence to our experimental findings. In the unlikely case of interacting spins, further effects should emerge, such as a resistive hysteresis as a function of the magnetic field.

There is the possibility that due to the large charge carrier density, our sample might be either in the strong localization regime or in the transition between weak and strong localization, allowing several contributions to the MR, with both negative and positive sign.[15]

Next we consider diffusive scattering at defects that should be highly enhanced by the nitrogen atoms that are distributed in the carbon lattice.[37,39] The magnetic field applied perpendicularly to the sample

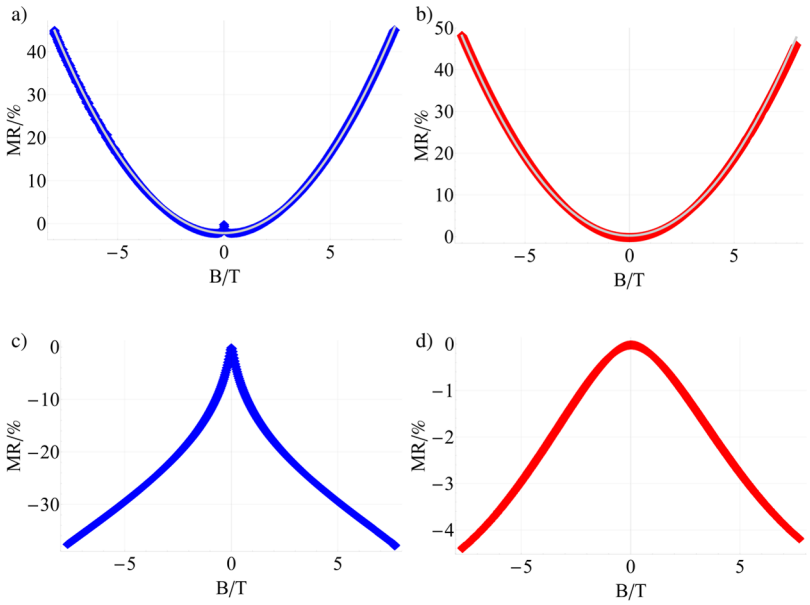

Figure 3. Magnetoresistance for doped and undoped graphene (magnetic fields applied perpendicular to the sample) for different temperatures. The upper line shows the undoped case for 2.3 K (a) and 279 K (b). At low temperature the weak localization peak is clearly visible at zero field. Classical Lorentz magnetoresistance, according to eq 4 is fitted to the data (white lines). Graphs (c) and (d) show the same measurements for the doped case where the sign and the shape of the curves change compared to the pristine graphene.

plane forces the charge carriers to follow a cyclotron trajectory with a radius given by[40]

$$r_c = \frac{\hbar\sqrt{n\pi}}{Be} \tag{5}$$

Higher magnetic fields lead to smaller radii and thus to less scattering at defect boundaries, increasing the mean free path and decreasing the resistance. The resulting radius for the doped graphene sample measures a few μm at a magnetic field of 0.1 T.

The magnitude of the effect will increase with decreasing temperature, just as observed for our nitrogen-doped graphene sample. However, the theoretical calculations predict a magnetoresistance that depends on the square of the magnetic field, while we observe a roughly linear dependence of the MR at higher fields for both room temperature and low temperatures.[39,41]

While no single model explains our observation, the superposition of different mechanisms can lead to negative linear MR. Following the approach of Zhang *et al.*[41] weak localization and diffusive boundary scattering in a certain superposition may result in a linear, negative MR, where the weights of the superposition are temperature dependent. So such a superposition can describe our low temperature observation well. For the high temperature measurement, weak localization is not expected to contribute significantly, and as a consequence a linear MR combined with weak localization does not fit our data at 279 K.

Altogether some of our data can be explained by the superposition of different effects. However, no theory is able to explain the low and high temperature regime calling for further work to describe a linear negative MR in a nitrogen-doped graphene system at all temperatures.

Finally we quantify the change in the charge transport with doping by analyzing the phase coherent transport at low temperatures and low fields. As already mentioned above, both low temperature MR signals exhibit a peak at small fields. As the signal is absent in the room temperature measurements (the MR flattens at 279 K when approaching small fields), this is a sign of quantum transport properties that is an established effect to determine transport properties quantitatively. We start with a basic model to describe weak localization, which allows one to easily understand the effect. Considering graphene as a 2D metal, one can describe the MR effect by

$$\Delta R(B) = -\frac{2e^2\rho_s^2}{\pi h}[F(dB\tau_\phi) - F(dB\tau)] \tag{6}$$

where d is defined by $d = (\hbar/4eD)$, $D = 0.3$ m^2/s is the diffusion constant,[42] $F(z)$ is given by $F(z) = \ln(z) + \Psi(1/2 + 1/z)$, and $\Psi(z)$ is the digamma function.[43] This description of weak localization rests on only two parameters, the phase coherence time τ_ϕ and the scattering time τ. The interplay between these two time scales leads to a reduction in the resistance for applied fields: the phase coherent transport is reduced due to applied fields as the field leads to an additional phase for charge carriers moving in the system which reduces the wave interference effect, thus leading to an increase of the resistivity at low fields. Note that this effect is most pronounced in low dimensional systems (such as graphene) where the charge carriers have

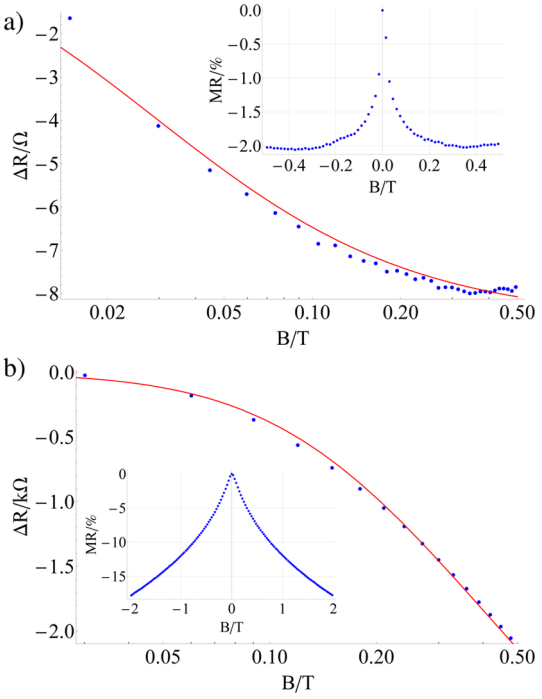

Figure 4. Fit of eq 6 for the magnetoresistance of undoped graphene (a) and nitrogen-doped graphene (b). Insets show close-ups of Figure 3 (a) and (c) for small fields.

higher probabilities to intersect their own path as necessary for the interference effect to occur. As both time scales will be strongly temperature dependent, this effect is mostly only present at low temperatures. The expression $\Delta R(B)$ is defined by

$$\Delta R(B) = \rho_s(B) - \rho_{fit}(B) - (\rho_s(0) - \rho_{fit}(0)) \quad (7)$$

Here $\rho_s(B)$ is the sheet resistance, and $\rho_{fit}(B)$ is a fit to the low temperature sheet resistance in order to subtract background events which do not originate from weak localization events. In the case of undoped graphene we fit the Lorentz Magnetoresistance given in eq 4, whereas for the doped sample a linear field dependence was used to estimate the background events in line with the models described above.

We now fit our experimental curves for doped and undoped graphene using eq 6. As shown in Figure 4 we find excellent agreement between the observed field dependence and the model. For the undoped sample we obtain a phase coherence time $\tau_\phi = (0.33 \pm 0.01)$ ps and a scattering time of $\tau = (0.03 \pm 0.019)$ ps. In general these times are of the order of magnitude found for other graphene samples and a little lower for what is observed for high quality epitaxial graphene.[43] This can be attributed to the fact that the transfer of the graphene films to the substrate leads to some strain and interaction with the substrate. A reduction of the times thus can be caused by adatoms, interaction with the substrate and other small defects, which we can also identify in the Raman spectrum of the undoped sample.

In case of the nitrogen-doped device we find, $\tau_\phi = (7.10 \pm 0.01)$ fs and $\tau = (6.30 \pm 0.01)$ fs. This drastic orders of magnitude decrease in the phase coherence time, and the scattering time shows the dominating effect of the doping on the charge carrier transport.[14] We attribute the decrease of both phase coherence time and scattering time to the nitrogen defects, which form additional scattering centers and thus decrease the mean free path of charge carriers. This quantitative result also explains the strongly reduced mobility of the charge carriers that we measure for nitrogen-doped graphene compared to undoped graphene and shows that we obtain a consistent picture of the effect of doping on the charge carrier transport in graphene.

CONCLUSION

We demonstrated the significant impact of nitrogen doping on the charge transport and magnetoresistance in graphene. Samples of doped and undoped graphene are fabricated by identical CVD and transfer processes to compare the effects of the doping while keeping the fabrication identical. Charge transport measurements at variable temperature performed on undoped CVD-graphene allow us to compare the results obtained for nitrogen-doped graphene. The measurements reveal a 6-fold increase of the charge carrier density due to the doping. Furthermore, the strong temperature dependence of the resistance is reminiscent of semiconductors, and fitting with the Mott variable range hopping model shows an opened band gap through the doping process as necessary for applications.

A positive and largely temperature-independent high field MR is found for undoped graphene which is attributed to Lorentz magnetoresistance. In contrast, a negative MR is observed for doped graphene at both 2.3 and 279 K, showing a clear temperature dependence. The latter can be partly explained with a superposition of defect boundary scattering due to the induced disorder and phase coherent transport.

For low fields and low temperatures, we observe a strongly increasing negative MR for both doped and undoped graphene due to quantum transport phenomena. A fit of the observed signals with a weak localization model yields excellent agreement. The deduced transport coherence times, which are directly correlated to the amount of defect scattering centers, are orders of magnitude reduced in doped graphene compared to undoped graphene, which allows us to conclude that the dopants act as effective scattering centers.

Together, the transport properties, the MR, and the quantum transport allow us to quantify the impact of the dopant on the charge carrier transport. The doping consistently increases the charge carrier density, opens a band gap, reverses the magnetoresistance, and reduces the scattering and coherence times by

orders of magnitude. Given the identical fabrication processes, we can attribute all these observed effects unambiguously to the additional dopants in the graphene, showing that nitrogen doping is a viable route for effectively tailoring the charge transport in doped graphene.

EXPERIMENTAL SECTION

The fabrication of all our samples has been carried out employing well-established techniques as follows. Nitrogen-doped graphene as well as undoped graphene are grown by CVD on copper foil,[26] yielding well-defined nitrogen dopants that are incorporated in the graphene lattice[17,44] as confirmed by Raman spectroscopy. Using a standard method,[45] the graphene is then transferred to substrates consisting of p-doped Si covered by 300 nm of SiO_2. The substrate is already prepared with contact pads for the electrical characterization, which are placed in a van der Pauw geometry.[46] The Au/Cr-pads placed at a distance of 100−800 μm are fabricated by electron beam lithography. For the transfer process, PMMA is spun onto graphene to protect it from the further treatment. Copper is etched away by iron(III) nitrate (concentration 1:20 mass parts), and the resulting solution is exchanged with ultra pure water. The residual film of graphene covered with PMMA is now transferred onto the substrate. The resulting device is dried, and the PMMA is removed by acetone. By Raman spectroscopy we analyze the defect structure and number of layers. Charge transport properties such as magnetoresistance and sheet resistance as well as charge carrier densities and mobilities are measured in a He^4 bath cryostat where uniaxial magnetic fields of up to 8 T are applied. A probe current of 20 μA has been used throughout the measurements.

Conflict of Interest: The authors declare no competing financial interest.

Acknowledgment. This work was funded by MoQuaS (Moquas Molecular Quantum Spintronics FP7-ICT-2013-10), the European Research Council through the Starting Independent Researcher Grant MASPIC (ERC-2007-StG 208162), the Advanced Grant NANOGRAPH, the Graphene Flagship (CNECT-ICT-604391) and the DFG (Schwerpunktprogramm 1459 Graphene).

Supporting Information Available: Additional figure showing the temperature dependence of the sheet resistance over the entire temperature range. While being exponential for high temperatures it becomes logarithmic for low temperatures as expected for weak localization. This material is available free of charge *via* the Internet at http://pubs.acs.org

REFERENCES AND NOTES

1. Morozov, S. V.; Novoselov, K. S.; Katsnelson, M. I.; Schedin, F.; Elias, D. C.; Jaszczak, J. A.; Geim, A. K. Giant Intrinsic Carrier Mobilities in Graphene and Its Bilayer. *Phys. Rev. Lett.* **2008**, *100*, 016602.
2. Chen, J. H.; Jang, C.; Xiao, S.; Ishigami, M.; Fuhrer, M. S. Intrinsic and Extrinsic Performance Limits of Graphene Devices on SiO_2. *Nat. Nanotechnol.* **2008**, *3*, 206–209.
3. Wang, Y.; Shao, Y.; Matson, D. W.; Li, J.; Lin, Y. Nitrogen-Doped Graphene and Its Application in Electrochemical Biosensing. *ACS Nano* **2010**, *4*, 1790–1798.
4. Stauber, T.; Peres, N. M. R.; Guinea, F. Electronic Transport in Graphene: A Semiclassical Approach Including Midgap States. *Phys. Rev. B* **2007**, *76*, 205423.
5. Wehling, T. O.; Katsnelson, M. I.; Lichtenstein, A. I. Adsorbates on graphene: Impurity States and Electron Scattering. *Chem. Phys. Lett.* **2009**, *476*, 125–134.
6. Cheng, S.-H.; Zou, K.; Okino, F.; Gutierrez, H. R.; Gupta, A.; Shen, N.; Eklund, P. C.; Sofo, J. O.; Zhu, J. Reversible Fluorination of Graphene: Evidence of a Two-Dimensional Wide Bandgap Semiconductor. *Phys. Rev. B* **2010**, *81*, 205435.
7. Robinson, J. P.; Schomerus, H.; Oroszlány, L.; Fal'ko, V. I. Adsorbate-Limited Conductivity of Graphene. *Phys. Rev. Lett.* **2008**, *101*, 196803.
8. Deifallah, M.; McMillan, P. F.; Corà, F. Electronic and Structural Properties of Two-Dimensional Carbon Nitride Graphenes. *J. Phys. Chem. C* **2008**, *112*, 5447–5453.
9. Martins, T. B.; Miwa, R. H.; da Silva, A. J. R.; Fazzio, A. Electronic and Transport Properties of Boron-Doped Graphene Nanoribbons. *Phys. Rev. Lett.* **2007**, *98*, 196803.
10. Cervantes-Sodi, F.; Csányi, G.; Piscanec, S.; Ferrari, A. C. Edge-Functionalized and Substitutionally Doped Graphene Nanoribbons: Electronic and Spin Properties. *Phys. Rev. B* **2008**, *77*, 165427.
11. Calandra, M.; Mauri, F. Electronic Structure of Heavily Doped Graphene: The Role of Foreign Atom States. *Phys. Rev. B* **2007**, *76*, 161406(R).
12. Roldán, R.; López-Sancho, M. P.; Guinea, F. Effect of Electron-Electron Interaction on the Fermi Surface Topology of Doped Graphene. *Phys. Rev. B* **2008**, *77*, 115410.
13. Wehling, T. O.; Novoselov, K. S.; Morozov, S. V.; Vdovin, E. E.; Katsnelson, M. I.; Geim, A. K.; Lichtenstein, A. I. Molecular Doping of Graphene. *Nano Lett.* **2008**, *8*, 173–177.
14. Moser, J.; Tao, H.; Roche, S.; Alzina, F.; Sotomayor Torres, C. M.; Bachtold, A. Magnetotransport in Disordered Graphene Exposed to Ozone: From Weak to Strong Localization. *Phys. Rev. B* **2010**, *81*, 205445.
15. Hong, X.; Cheng, S.-H.; Herding, C.; Zhu, J. Colossal Negative Magnetoresistance in Dilute Fluorinated Graphene. *Phys. Rev. B* **2011**, *83*, 085410.
16. Venugopal, A.; Chan, J.; Li, X.; Magnuson, C. W.; Kirk, W. P.; Colombo, L.; Ruoff, R. S.; Vogel, E. M. Effective Mobility of Single-Layer Graphene Transistors as a Function of Channel Dimensions. *J. Appl. Phys.* **2011**, *109*, 104511.
17. Wei, D.; Liu, Y.; Wang, Y.; Zhang, H.; Huang, L.; Yu, G. Synthesis of N-Doped Graphene by Chemical Vapor Deposition and Its Electrical Properties. *Nano Lett.* **2009**, *9*, 1752–1758.
18. Lv, R.; Li, Q.; Botello-Méndez, A. R.; Hayashi, T.; Wang, B.; Berkdemir, A.; Hao, Q.; Elías, A. L.; Cruz-Silva, R.; Gutiérrez, H. R.; et al. Nitrogen-Doped Graphene: Beyond Single Substitution and Enhanced Molecular Sensing. *Sci. Rep.* **2012**, *2*, 586.
19. Graf, D.; Molitor, F.; Ensslin, K.; Stampfer, C.; Jungen, A.; Hierold, C.; Wirtz, L. Spatially Resolved Raman Spectroscopy of Single- and Few-Layer Graphene. *Nano Lett.* **2007**, *7*, 238–242.
20. Ni, Z.; Wang, Y.; Yu, T.; Shen, Z. Raman Spectroscopy and Imaging of Graphene. *Nano Res.* **2008**, *1*, 273–291.
21. Gupta, A.; Chen, G.; Joshi, P.; Tadigadapa, S.; Eklund, P. C. Raman Scattering from High-Frequency Phonons in Supported n-Graphene Layer Films. *Nano Lett.* **2006**, *6*, 2667–2673.
22. Das, A.; Pisana, S.; Chakraborty, B.; Piscanec, S.; Saha, S. K.; Waghmare, U. V.; Novoselov, K. S.; Krishnamurthy, H. R.; Geim, A. K.; Ferrari, A. C.; et al. Monitoring Dopants by Raman Scattering in an Electrochemically Top-Gated Graphene Transistor. *Nat. Nanotechnol.* **2008**, *3*, 210–215.
23. Malard, L. M.; Pimenta, M. A.; Dresselhaus, G.; Dresselhaus, M. S. Raman Spectroscopy in Graphene. *Phys. Rep.* **2009**, *473*, 51–87.
24. Ferrari, A. C. Raman Spectroscopy of Graphene and Graphite: Disorder, ElectronUPhonon Coupling, Doping and Nonadiabatic Effects. *Solid State Commun.* **2007**, *143*, 47–57.
25. Casiraghi, C.; Pisana, S.; Novoselov, K. S.; Geim, A. K.; Ferrari, A. C. Raman Fingerprint of Charged Impurities in Graphene. *Appl. Phys. Lett.* **2007**, *91*, 233108.
26. Ito, Y.; Christodoulou, C.; Nardi, M. V.; Koch, N.; Sachdev, H.; Müllen, K. Chemical Vapor Deposition of N-Doped Graphene and Carbon Films: The Role of Precursors and Gas Phase. *ACS Nano* **2014**, *8*, 3337–3346.

27. Bolotin, K. I.; Sikes, K. J.; Jiang, Z.; Klima, M.; Fudenberg, G.; Hone, J.; Kim, P.; Stormer, H. L. Ultrahigh Electron Mobility in Suspended Graphene. *Solid State Commun.* **2008**, *146*, 351–355.
28. Dean, C. R.; Young, A. F.; Meric, I.; Lee, C.; Wang, L.; Sorgenfrei, S.; Watanabe, K.; Taniguchi, T.; Kim, P.; Shepard, K. L.; Hone, J. Boron Nitride Substrates for High-Quality Graphene Electronics. *Nat. Nanotechnol.* **2010**, *5*, 722–726.
29. Tan, Y.-W.; Zhang, Y.; Bolotin, K.; Zhao, Y.; Adam, S.; Hwang, E. H.; Das Sarma, S.; Stormer, H. L.; Kim, P. Measurement of Scattering Rate and Minimum Conductivity in Graphene. *Phys. Rev. Lett.* **2007**, *99*, 246803.
30. Song, H. S.; Li, S. L.; Miyazaki, H.; Sato, S.; Hayashi, K.; Yamada, A.; Yokoyama, N.; Tsukagoshi, K. Origin of the Relatively Low Transport Mobility of Graphene Grown Through Chemical Vapor Deposition. *Sci. Rep.* **2012**, *2*, 337.
31. Li, X.; Cai, W.; An, J.; Kim, S.; Nah, J.; Yang, D.; Piner, R.; Velamakanni, A.; Jung, I.; Tutuc, E.; et al. Large-Area Synthesis of High-Quality and Uniform Graphene Films on Copper Foils. *Science* **2009**, *324*, 1312–1314.
32. Wang, H.; Thandavarayan, M.; Wang, X. Review on Recent Progress in Nitrogen-Doped Graphene: Synthesis, Characterization, and Its Potential Applications. *ACS Catal.* **2012**, *2*, 781–794.
33. Wang, F.; Liu, G.; Rothwell, S.; Nevius, M.; Tejeda, A.; Taleb-Ibrahimi, A.; Feldman, L. C.; Cohen, P. I.; Conrad, E. H. Wide-Gap Semiconducting Graphene from Nitrogen-Seeded SiC. *Nano Lett.* **2013**, *13*, 4827–4832.
34. Mott, N. F. Conduction in Non-Crystalline Materials. *Philos. Mag.* **1969**, *19*, 835–852.
35. Kohler, M. Zur Magnetischen Widerstandsänderung Reiner Metalle. *Ann. Phys.* **1938**, *424*, 211–218.
36. Tongay, S.; Berke, K.; Lemaitre, M.; Nasrollahi, Z.; Tanner, D. B.; Hebard, A. F.; Appleton, B. R. Stable Hole Doping of Graphene for Low Electrical Resistance and High Optical Transparency. *Nanotechnology* **2011**, *22*, 425701.
37. Zhou, Y.-B.; Han, B.-H.; Liao, Z.-M.; Wu, H.-C.; Yu, D.-P. From Positive to Negative Magnetoresistance in Graphene with Increasing Disorder. *Appl. Phys. Lett.* **2011**, *98*, 222502.
38. Rappoport, T. G.; Uchoa, B.; Castro Neto, A. H. Magnetism and Magnetotransport in Disordered Graphene. *Phys. Rev. B* **2009**, *80*, 245408.
39. Fujita, S. Negative Magnetoresistance in Carbons and Diffuse Scattering at Crystallite Boundaries. *Carbon* **1968**, *6*, 746–748.
40. Mayorov, A. S.; Gorbachev, R. V.; Morozov, S. V.; Britnell, L.; Jalil, R.; Ponomarenko, L. A.; Blake, P.; Novoselov, K. S.; Watanabe, K.; Taniguchi, T.; et al. Micrometer-Scale Ballistic Transport in Encapsulated Graphene at Room Temperature. *Nano Lett.* **2011**, *11*, 2396–2399.
41. Zhang, X.; Xue, Q. Z.; Zhu, D. D. Positive and Negative Linear Magnetoresistance of Graphite. *Phys. Lett. A* **2004**, *320*, 471–477.
42. Berger, C.; Song, Z.; Li, X.; Wu, X.; Brown, N.; Naud, C.; Mayou, D.; Li, T.; Hass, J.; Marchenkov, N.; et al. Electronic Confinement and Coherence in Patterned Epitaxial Graphene. *Science* **2006**, *312*, 1191–1196.
43. Wu, X.; Li, X.; Song, Z.; Berger, C.; de Heer, W. A. Weak Antilocalization in Epitaxial Graphene: Evidence for Chiral Electrons. *Phys. Rev. Lett.* **2007**, *98*, 136801.
44. Zhao, L.; He, R.; Rim, K. T.; Schiros, T.; Kim, K. S.; Zhou, H.; Gutiérrez, C.; Chockalingam, S. P.; Arguello, C. J.; Pálová, L.; et al. Visualizing Individual Nitrogen Dopants in Monolayer Graphene. *Science* **2011**, *333*, 999–1003.
45. Li, X.; Zhu, Y.; Cai, W.; Borysiak, M.; Han, B.; Chen, D.; Piner, R. D.; Colombo, L.; Ruoff, R. S. Transfer of Large-Area Graphene Films for High-Performance Transparent Conductive Electrodes. *Nano Lett.* **2009**, *9*, 4359–4363.
46. van der Pauw, J. A Method of Measuring Specific Resistivity and Hall Effect of Discs of Arbitrary Shape. *Philips Res. Rep.* **1958**, *13*, 1–9.